RESEARCH PAPER

PCCP
www.rsc.org/pccp

Hybrid Langmuir–Blodgett monolayers containing clay minerals: effect of clay concentration and surface charge density on the film formation

Robin H. A. Ras,[a] József Németh,[ab] Cliff T. Johnston,[c] Elaine DiMasi,[d] Imre Dékány[b] and Robert A. Schoonheydt*[a]

[a] *Centrum voor Oppervlaktechemie en Katalyse, K.U.Leuven, Kasteelpark Arenberg 23 B-3001, Leuven, Belgium. E-mail: robert.schoonheydt@agr.kuleuven.ac.be*
[b] *Department of Colloid Chemistry, University of Szeged, Aradi V. t. 1. H-6720, Szeged, Hungary*
[c] *Birck Nanotechnology Center, 915 W. State Street, 1150 LILY Hall, Purdue University, West Lafayette IN 47907-2054, USA*
[d] *National Synchrotron Light Source Department, Brookhaven National Laboratory, Upton NY 11973-5000, USA*

Received 20th April 2004, Accepted 11th June 2004
First published as an Advance Article on the web 28th June 2004

To control the properties of hybrid organo-clay films prepared by the Langmuir–Blodgett (LB) method, the film formation mechanism should be understood. This work aimed to understand what occurs at the air–water interface after the spreading of cationic surfactants (octadecyl rhodamine B, 3,3′-dioctadecyl oxacarbocyanine) on aqueous dispersions of smectite clay minerals (saponite, montmorillonite, hectorite, laponite), resulting in hybrid organo-clay films. Information on the amount of surfactant molecules and clay particles in the hybrid films was obtained with surface pressure *versus* molecular area isotherms, attenuated total reflection infrared spectroscopy, ultraviolet-visible spectroscopy and atomic force microscopy. X-ray reflectivity measurements indicated that the surfactant molecules had adsorbed on only one side of the clay mineral lamella. With increasing clay concentration of the dispersion, the isotherms shifted to a lower lift-off area, a minimum lift-off area (MLA) was reached and then the lift-off area increased again. Films made at lower than the MLA clay concentration consisted of two phases: an organic phase and a hybrid organo-clay phase. Films made at the MLA clay concentration consisted of dense monolayers of the surfactant molecules and single clay mineral lamellae. The density of the surfactant molecules was highly correlated with the surface charge density of the clay minerals. These films had low water content. Films made at higher than the MLA clay concentration contained less surfactant, aggregates of the clay mineral particles, residual Na^+ ions and water. With the clay concentration of the dispersion and the surface charge density of the clay mineral, the properties of hybrid organo-clay LB films can be adjusted.

1. Introduction

Nanostructured materials have gained worldwide interest because they may exhibit valuable properties for potential optical, electronic or sensor applications.[1–4] They often require a hierarchical organization from the molecular to the macroscopic scale. One approach is to use organic molecules and inorganic nanoparticles as building blocks to create hybrid structures of increasing complexity.[5] The successive deposition of ultrathin films containing nanoparticles is a viable way towards the construction of complex three-dimensional structures.[6] The high aspect ratio and the chemical properties of clay mineral particles make them interesting as nanosized building blocks.[7,8]

Two levels of organization can be considered in materials containing clay minerals and adsorbed molecules: the organization of the molecules on the clay mineral surface and the organization of the clay mineral lamellae in layers.

A lamella of swelling clay minerals (or smectites) is defined in this paper as the arrangement of two tetrahedral sheets that sandwich an octahedral sheet with a combined thickness of less than one nanometer. The atoms within the same lamella are held together by covalent bonds, making a lamella the elementary structure of clay minerals. Clay mineral particles mostly consist of stacks of these lamellae. Most clay scientists generally refer to the elementary structure of clay minerals as a 'layer'.[9] The term 'lamella' is used in this paper because the term 'layer' can give confusion when clay mineral lamellae are deposited in a layer or film.

Two methods have been explored to prepare nanostructured materials that consist of single clay mineral lamellae: layer-by-layer self-assembly and Langmuir–Blodgett. Layer-by-layer self-assembly is a simple method to construct layered materials containing single clay mineral lamellae.[7,8] The control over the three-dimensional structure is limited, however. The Langmuir–Blodgett (LB) method allows a higher degree of control on the film structure. In 1994, two research groups independently reported on hybrid clay films prepared by spreading organo-clay complexes dispersed in organic solvents at the air–water interface.[10,11] This method, however, did not allow the preparation of single clay mineral lamellae. In 1999, a different approach was used where cationic surfactants are spread at the air–water interface of a clay mineral dispersion. In this approach the clay particles are allowed to adsorb from the dispersion onto the surfactant monolayer.[12,13] The incorporation of single lamellae of clay minerals becomes possible *via* this method and multilayered hybrid structures have been prepared by successive depositions.[14,15]

DOI: 10.1039/b405862c

 This journal is © The Owner Societies 2004

The clay concentration influences significantly the properties of the hybrid monolayer.[14–16] Surface pressure *versus* molecular area (Π–a) isotherms exhibit a shift in the lift-off area and compressibility when the clay concentration is varied.[14–16] For low clay concentrations (<5 mg dm^{-3} in the case of octadecylammonium monolayers) the lift-off area shifts to lower values than for water; for high clay concentrations the shift is to higher lift-off areas.[14,16] Umemura *et al.* investigated octadecylammonium hybrid monolayers by infrared spectroscopy and observed the molecular density to decrease with increasing clay concentration.[16] The effect of clay concentration on the monolayer properties have not been explained adequately.

The mechanism for film formation should be known in more detail to achieve a better control on the organization of molecules and particles in hybrid organo-clay films. This work aims to understand the phenomena that occur at the air–water interface after spreading cationic surfactants on a clay mineral dispersion. It is recognized that the surface charge density of the clay minerals controls the surfactant organization in the monolayer.

Recently, we reported on attenuated total reflection Fourier-transform infrared (ATR-FTIR) spectroscopy to study the clay part of the films.[17] In the current work, the ATR-FTIR technique is used to analyse the cationic surfactant as well. Molecular densities are determined using Π–a isotherms, ATR-FTIR spectroscopy and UV-Vis spectroscopy. The clay content is determined using Π–a isotherms, atomic force microscopy and ATR-FTIR spectroscopy. The combined analysis of both the clay mineral and the surfactant allows an analysis of the hybrid film formation process. The analysis is confirmed qualitatively by X-ray reflectivity measurements.

2. Materials and methods

2.1. Clay minerals

The clay mineral species used in this work were saponite (SapCa-1), Arizona montmorillonite (SAz-1), hectorite (SHCa-1), obtained from the Source Clays Repository of the Clay Minerals Society, and laponite RD obtained from Laporte Inorganics, UK. Laponite RD was used as received. The other clay minerals were Na^+ saturated by repeated (three times) exchange with 1 molar NaCl solutions followed by dialysis with water until a negative Cl^- test was obtained using $AgNO_3$. The particle size fraction between 0.5 and 2.0 μm was obtained by centrifugation and freeze-drying of a salt-free, Na^+ exchanged clay mineral dispersion. Characteristics of the clay minerals are shown in Table 1.

2.2. Molecules

Octadecyl rhodamine B chloride (RhB18, Molecular Probes) and 3,3′-dioctadecyl oxacarbocyanine perchlorate (OXA18, Fluka) were used as received and were dissolved in HPLC-grade chloroform (99.9%, Aldrich, stabilized by 0.5–1% ethanol) to prepare a spreading solution of respectively 9.11×10^{-4} mol dm^{-3} and 1×10^{-3} mol dm^{-3}.

2.3. Film preparation

LB films were prepared on a NIMA Technology model 611 LB trough at a temperature of 23 ± 1 °C. Clay dispersions stirred for 24 h in Milli-Q water were used as the subphase. The clay concentration ranged from 2 to 250 mg dm^{-3}. A microsyringe was used to spread 40 μl of the dye dissolved in chloroform over the subphase. After 15 min, the film was compressed at a rate of 30 cm^2 min^{-1}. Films were deposited in upstroke (lifting speed of 5 mm min^{-1}) on ZnSe internal reflection elements (IREs) at surface pressures of 2 mN m^{-1} and 15 mN m^{-1} and on glass substrates and on silicon wafers at a surface pressure of 10 mN m^{-1}. The IREs were cleaned prior to each deposition by gently rubbing with a paper tissue soaked in methanol. The glass substrates and silicon wafers were cleaned in piranha solution (mixture of 70 ml concentrated H_2SO_4 and 30 ml 35% H_2O_2) for 30 min at 90 °C. Subsequently the substrates were thoroughly rinsed by deionized water and stored in Milli-Q water no longer than 30 days.

2.4. Infrared spectroscopy

The IREs were ZnSe trapezoidal-shaped crystals (Spectroscopy Central, UK) (50 mm × 20 mm × 2 mm) with 25 internal reflections and were measured in a vertical ATR cell using a Bruker IFS66v/S vacuum FTIR spectrometer with an operating vacuum lower than 3 mbar inside the spectrometer. Because the IRE was not covered with film where it was attached to the dipper, there are only 24 active reflections. Polarized ATR-FTIR spectra were obtained using a wire-grid polarizer. The FTIR spectrometer was equipped with a liquid nitrogen cooled MCT detector and a KBr/Ge beam splitter. A total of 512 scans were signal averaged using an optical resolution of 2 cm^{-1}. Spectra were analyzed with Grams/32 AI software (version 6.00).

2.5. Ultraviolet-visible (UV-Vis) spectroscopy

The UV-Vis absorption spectra of the monolayers on glass substrates were measured from 400 nm to 700 nm on a Perkin Elmer Lambda 12 spectrometer. A clean glass slide was used as reference for the films. The monomer spectrum of the adsorbed RhB18 species is calculated from the monomer spectrum in solution. Monomer species of Rh3B (similar structure as RhB18 but with ethyl group instead of octadecyl) in dilute ethanolic solution[18] and on saponite in aqueous dispersion[19] have maxima at 556 nm and 567 nm respectively. As the monomer spectrum of RhB18 in ethanol (10^{-6} mol dm^{-3}) has its maximum at 556 nm, we can assume the monomer of RhB18 on the saponite surface to have its maximum at 567 nm. The spectrum of RhB18 in ethanol is first converted to wavenumbers, then the spectrum is shifted so that the maximum is at 17 637 cm^{-1}. Conversion to wavelength gets the monomer spectrum of RhB18 on saponite with $\lambda_{max} = 567$ nm used for the calculation of the dimer spectrum. To calculate the dimer spectra of RhB18 films, the calculated monomer spectrum is subtracted from the measured spectra of the films *via*

Table 1 Properties of clay minerals

Clay mineral species	Composition of half a unit cell	Unit cell dimensions $a \times b$
SapCa-1 saponite	[a] $[(Si^{4+}_{3.57}Al^{3+}_{0.38}Fe^{3+}_{0.05})(Mg^{2+}_{3.00})O_{10}(OH)_2]M^+_{0.43}$	[b] 5.33 Å × 9.23 Å
SAz-1 montmorillonite	[c] $[(Si^{4+}_{4.00})(Al^{3+}_{1.37}Mg^{2+}_{0.58}Fe^{3+}_{0.07}Mn^{2+}_{0.01}Ti^{4+}_{0.01})O_{10}(OH)_2]M^+_{0.47}$	[d] 5.18 Å × 9.00 Å
SHCa-1 hectorite	[c] $[(Si^{4+}_{3.96}Al^{3+}_{0.04})(Mg^{2+}_{2.68}Li^+_{0.28}\ Al^{3+}_{0.01}Fe^{3+}_{0.01})O_{10}(OH)_2]M^+_{0.34}$	[d] 5.25 Å × 9.18 Å
Laponite RD	[e] $[(Si^{4+}_{4.00})(Mg^{2+}_{2.67}Li^+_{0.33})O_{10}(OH)_2]Na^+_{0.33}$	—

[a] Chemical analysis by ICP-OES (inductively coupled plasma-optical emission spectrometry) *via* nebulization of aqueous clay mineral dispersions. The composition compares with the data supplied by the Clay Minerals Society.[46] [b] Determined by XRD analysis. The unit cell dimensions agree with the values obtained for the Kozákov saponite.[47] [c] Ref. 48. [d] Ref. 38. [e] Ref. 49.

the tool 'spectral subtract–autosubtract' in the Grams/32 AI software (version 6.00). This automated subtraction procedure is based on an iterative algorithm which calculates the subtraction factor by minimizing the derivative of the residual spectrum.[20]

2.6. Atomic force microscopy

Atomic force microscopy images of the monolayers on glass slides were obtained on a Topometrix Discoverer system TMX 2010 with a Si_3N_4 tip in contact mode (spring constant = 0.032 mN m^{-1}).

2.7. X-ray reflectivity

X-ray reflectivity measurements were performed at Beamline X22A at the National Synchrotron Light Source on 20 mm long silicon wafers in air, using an X-ray wavelength of 1.155 Å. Measurements were repeated at different locations on each sample surface to ensure that beam damage was not a factor. Reflectivity data was acquired with a Bicron single channel detector. The off-specular background was measured both within and normal to the scattering plane. The experimental reflectivities were normalized by the Fresnel reflectivity calculated for silicon and fit to one- or two-box models designating slabs of homogeneous electron density with Gaussian smoothing between layers. Data were fit in the kinematic limit for q_z values greater than 5–10 times the critical angle q_c for silicon.

3. Results

3.1. Surface pressure *versus* molecular area isotherms

The surface pressure *versus* molecular area (Π–a) isotherms of octadecyl rhodamine B (RhB18) monolayers on saponite, montmorillonite, hectorite and laponite dispersions are shown in Fig. 1(a–d). Π–a isotherms of 3,3′-dioctadecyl oxacarbocyanine (OXA18) monolayers on saponite and hectorite dispersions are shown in Fig. 2(a–b).

On water, in the absence of clay minerals, the Π–a isotherm is a smoothly increasing curve with a lift-off area of 168 $Å^2$ for RhB18 and 139 $Å^2$ for OXA18 (the lift-off area is determined according to the method described in the Appendix). Lift-off areas of these compounds have not been reported yet. However, the molecular areas of 88 $Å^2$ at 20 mN m^{-1} and 63 $Å^2$ at 30 mN m^{-1} for the RhB18 monolayer on water compare favourably with the values of 80 $Å^2$ at 20 mN m^{-1} and 60 $Å^2$ at 30 mN m^{-1} reported by Vuorimaa *et al.*[21] Similarly, the molecular area of 60 $Å^2$ at 30 mN m^{-1} for the OXA18 monolayer on water compares favourably with the value of 65 $Å^2$ at 30 mN m^{-1} reported by Biesmans *et al.*[22]

Upon adding small amounts of clay minerals to the aqueous subphase, the lift-off area is shifted to lower values while retaining a similar shape to the water-only Π–a isotherm. Increasing the clay concentration further, however, results in the lift-off area shifting to higher values and the overall shape of the Π–a isotherm is altered. This behaviour is consistent with studies of octadecylammonium[14,16] and ruthenium(II) complexes[15] on saponite dispersions. For each of the four clay minerals studied, there is a clay concentration for which the lift-off area is a minimum. By recording isotherms on dispersions with varying clay concentration, the minimum lift-off area (MLA) is determined (Fig. 1(a–d); Fig. 2(a–b)).

The MLA of RhB18 and OXA18 hybrid monolayers, the amount of clay minerals in the aqueous dispersion corresponding to the MLA and the average area per charge in the clay mineral lattice are listed in Table 2. The amount of clay minerals in dispersion needed for MLA is ~50 mg dm^{-3} for the natural clay minerals (saponite, montmorillonite and hectorite) and ~10 mg dm^{-3} for laponite. This suggests that particle size plays a role in the formation of the hybrid clay film. The particle size of laponite is about 20 nm[23] while the natural clay minerals have sizes ranging from tens of nanometer up to micrometers.[8,14,15,17]

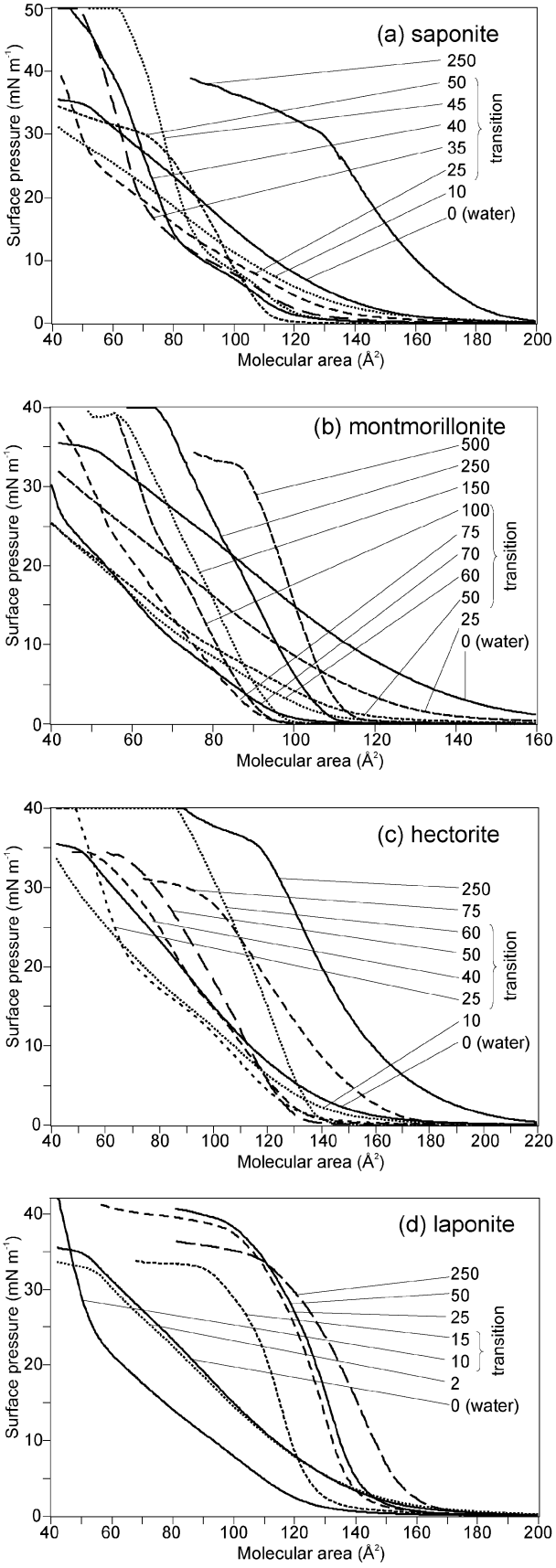

Fig. 1 Surface pressure *versus* molecular area (Π–a) isotherms of monolayers of RhB18 prepared on (a) saponite, (b) montmorillonite, (c) hectorite and (d) laponite clay mineral dispersions at different clay concentrations (mg dm^{-3}).

This journal is © The Owner Societies 2004

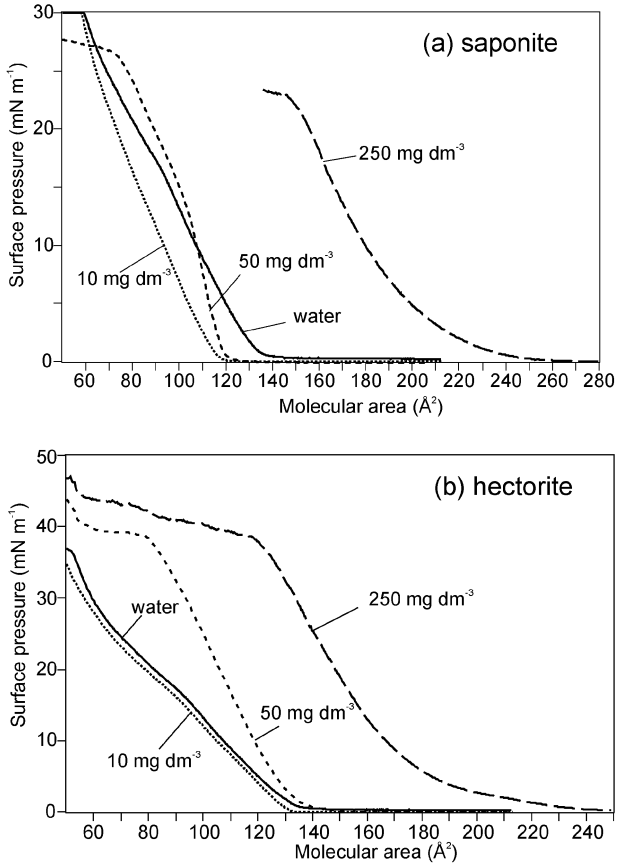

Fig. 2 Surface pressure *versus* molecular area (Π–a) isotherms of monolayers of OXA18 prepared on (a) saponite and (b) hectorite dispersions at different clay concentrations (mg dm^{-3}).

Table 2 Lift-off area of RhB18 and OXA18 monolayers on water and the minimum lift-off area (MLA) of RhB18 and OXA18 monolayers on clay mineral dispersions. The lift-off area is calculated according to the method in Appendix. The area per charge of the clay mineral is calculated from the charge deficit per unit cell and the unit cell dimensions listed in Table 1. It is assumed that the unit cell dimensions of laponite are similar to those of hectorite

Sub-phase	Clay concentration/mg dm^{-3}	MLA for RhB18 monolayers/Å^2	MLA for OXA18 monolayers/Å^2	Area per charge/Å^2
Water	0	168	139	—
SapCa-1	50	116	118	114
SAz-1	75	98	n.d.[a]	99
SHCa-1	50	137	132	142
Laponite RD	10	137	n.d.	146

[a] n.d. = not determined.

There is a clear one-to-one correspondence between the MLA and the average area per charge (= 1/surface charge density) of the clay mineral. It suggests that an ion-exchange reaction takes place between the clay mineral particles and the organic cations, resulting in a hybrid organo-clay monolayer at the air–water interface.

3.2. Apparent compressibilities

The apparent compressibility, C', is defined as

$$C' = -\frac{1}{a_1}\frac{a_2 - a_1}{\Pi_2 - \Pi_1} \quad (1)$$

where a_1 and a_2 correspond to the area per molecule at surface pressures of Π_1 and Π_2, respectively. Apparent compressibilities of the RhB18 isotherms on the different clay mineral dispersions are calculated according to eqn. (1) and are displayed in Fig. 3. Π_1 and Π_2 were chosen in the fairly straight section of the isotherms. The apparent compressibility depends on the type of clay mineral and on the amount of clay minerals in the dispersions. For saponite and montmorillonite, the apparent compressibility first increases with increasing clay concentration until a maximum is obtained around the clay concentration which gives the MLA. At higher clay concentration, the apparent compressibilities decrease to reach a minimum value in the range 7.5–13.4 m N^{-1}. Similar values have been obtained for octadecylammonium monolayers on saponite dispersions[14] and monolayers of ruthenium(II) complexes on saponite dispersions,[15] showing that the clay particles determine the compressibility of the film. In the case of monolayers prepared on saponite dispersions there is a clay concentration, 25–45 mg dm^{-3}, where the Π–a isotherms have a step that divides the isotherm in regions with different compressibility, one corresponding to the maximum C' of ~35 m N^{-1}, the second to the minimum C' of ~7.5 m N^{-1}. Steps in an isotherm indicate the coexistence of two phases with distinct properties.[24] The two phases that can be recognized here are the organic phase without clay and the hybrid organo-clay phase.

For hectorite and laponite, there is not a maximum in apparent compressibility with increasing clay concentration. The maximum value is that of RhB18 in the absence of clay. Addition of clay results in a decrease of the apparent compressibility until a minimum value is reached of ~12.5 m N^{-1} for hectorite, and of ~5 m N^{-1} for laponite.

3.3. Coexisting phases: linear increase in fraction *f* of the clay-containing hybrid phase

Our working hypothesis is now that (i) at clay concentrations below those corresponding to the MLA, a monolayer is formed containing two phases: an organic phase, consisting of the cationic surfactant, and a hybrid organo-clay phase, consisting of the cationic surfactant adsorbed onto a single clay mineral lamella; (ii) at clay concentrations corresponding to the MLA the film at the air–water interface is a hybrid organo-clay monolayer of which the molecular density corresponds to the surface charge density of the clay mineral surface; (iii) at clay concentrations above those corresponding to the MLA a clay film is formed in which the molecular density is reduced.

At low clay concentrations the monolayer consists of two coexisting phases: an organic phase and a hybrid organo-clay phase. The measured molecular area is then a linear combination of the molecular area of the hybrid organo-clay phase and the molecular area of organic phase according to:

$$\text{molecular area} = f \times \text{molecular area of organo-clay phase} + (1 - f) \times \text{molecular area of organic phase} \quad (2)$$

f is the fraction of the surface covered by the hybrid organo-clay phase and $(1 - f)$ is the fraction occupied by the organic phase. If the molecular area of the hybrid organo-clay phase equals the MLA (116 Å^2 for the RhB18–saponite monolayer) and if the molecular area of the organic phase equals the lift-off area of the pure organic monolayer (168 Å^2 for the RhB18 monolayer on water), then the fraction f can be calculated at lift-off and is shown in Fig. 4. One observes for the clay minerals under investigation a linear increase of fraction f with increasing clay concentration. The data show that the simple model of the coexistence of two phases is a good first approximation to hybrid film formation.

3.4. Atomic force microscopy analysis of clay mineral particles in the hybrid films

Atomic force microscopy (AFM) images of hybrid films containing OXA18 and saponite are shown in Fig. 5. Films

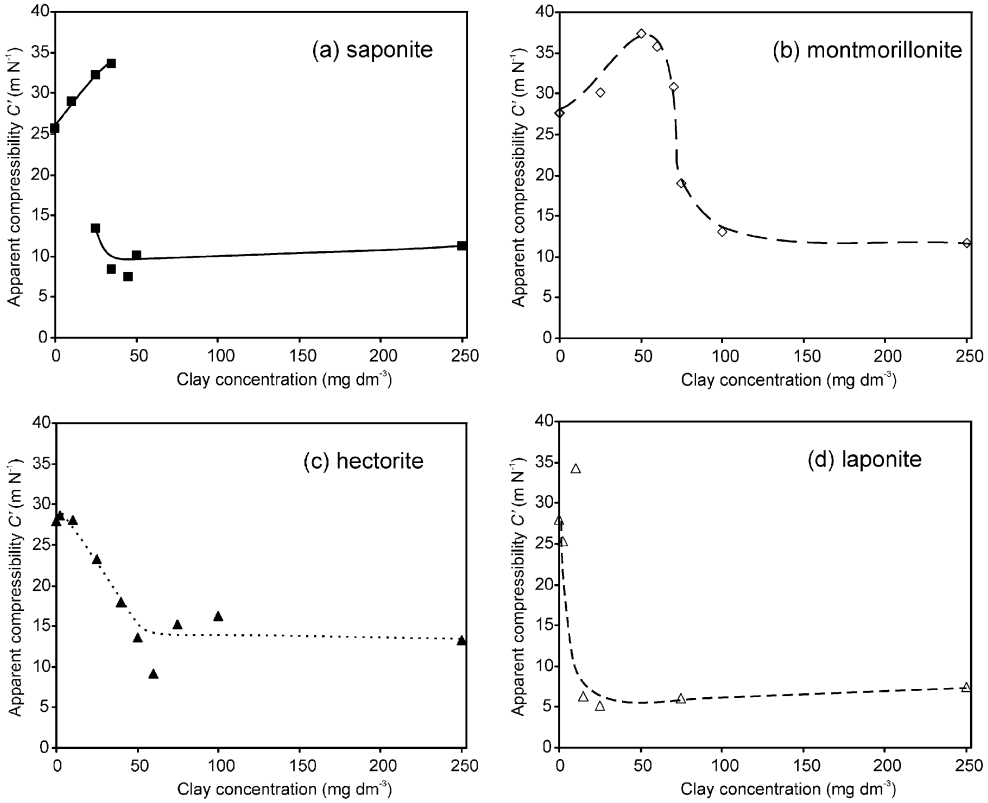

Fig. 3 Apparent compressibility C' determined from Π–a isotherms of the RhB18 monolayer on clay mineral dispersions of (a) saponite, (b) montmorillonite, (c) hectorite and (d) laponite.

were prepared at three different clay concentrations: (a) 10 mg dm^{-3}, (b) 50 mg dm^{-3} and (c) 250 mg dm^{-3} and deposited at a surface pressure of 10 mN m^{-1}. Plate-shaped particles of different sizes and shapes are observed, of which some overlap. At 10 mg dm^{-3}, the coverage by clay mineral particles is low, suggesting the presence of the organic phase and the hybrid organo-clay phase. The film prepared on a 50 mg dm^{-3} clay mineral dispersion contains significantly more particles. The surface is nearly completely covered with single clay mineral lamellae. The clay mineral lamellae are not in close contact as the particle edges are clearly visible. At higher clay concentration (250 mg dm^{-3}) the clay mineral particles make a nearly continuous film and the particle edges are less clear. A large particle, at least four clay mineral lamellae thick, is visible in the top-left corner.

The AFM images at least qualitatively confirm the simple model with the coexistence of two phases below the MLA clay concentration (10 mg dm^{-3}); a hybrid phase at the MLA clay concentration (50 mg dm^{-3}) and a hybrid phase with clay aggregates above the MLA clay concentration (250 mg dm^{-3}).

3.5. Infrared analysis of clay mineral particles in the hybrid films

ATR-FTIR spectra of the clay mineral particles in the film are taken for films deposited on ZnSe internal reflection elements. Typical results for RhB18–saponite films are given in Fig. 6. The inset shows the ATR-FTIR spectra with bands at 996 cm^{-1} and 1063 cm^{-1}, assigned respectively to the in-plane and out-of-plane Si–O stretching vibration, ν(Si–O). The 1063 cm^{-1} band intensity depends strongly on the polarization of light as expected for films in which the clay mineral particles have a preferential orientation parallel with the substrate. These spectral bands have been recently discussed in detail.[17,25] Here we use the intensity of the Si–O band at 996 cm^{-1} as a measure for the clay content in the film as a function of clay concentration in the dispersion for films deposited at 15 mN m^{-1} (black squares) and at 2 mN m^{-1} (white squares).

Below the MLA clay concentration (<50 mg dm^{-3} for saponite) the 996 cm^{-1} band intensity increases with clay concentration to reach a plateau around the MLA clay concentration and a moderate increase at higher clay concentration. The increase below the MLA clay concentration is consistent with the model as expressed by eqn. (2) and Fig. 4. More and more clay mineral particles adsorb and the hybrid organo-clay phase grows at the expense of the organic phase.

The plateau in the Si–O band intensity obtained for saponite concentrations 35–50 mg dm^{-3} corresponds to a monolayer of single clay mineral lamellae. The intensity of the monolayer at 15 mN m^{-1} is slightly higher than at 2 mN m^{-1}, except for the dip at 35 mg dm^{-3} at 2 mN m^{-1}. This dip is reproducible, but we have no explanation for it. The increasing clay content with increasing surface pressure has been observed by Umemura *et al.* using AFM for clay films containing ruthenium(II) complexes[15] and octadecylammonium cations.[14] Above the MLA clay concentration, more aggregates of clay mineral particles are incorporated in the hybrid film. This explains the moderate increase of the Si–O band intensity at 996 cm^{-1} from 50 to 250 mg dm^{-3}.

3.6. Density of surfactant molecules in the monolayers

The density of RhB18 molecules in the films can be determined from the Π–a isotherms, from the ATR-FTIR intensity of the 1590 cm^{-1} band of RhB18 (assigned to the ring CC stretching vibration[26]) and from the UV-Vis spectral intensities of RhB18. Representative data are shown in Fig. 7. The number of molecules per unit film area increases with amount of clay minerals in the dispersion to reach a maximum around 35 mg dm^{-3} at 15 mN m^{-1} (see Fig. 7a). Above 35 mg dm^{-3} the molecular density rapidly decreases. There are significantly less molecules per unit area in the film deposited at 2 mN m^{-1}.

This journal is © The Owner Societies 2004

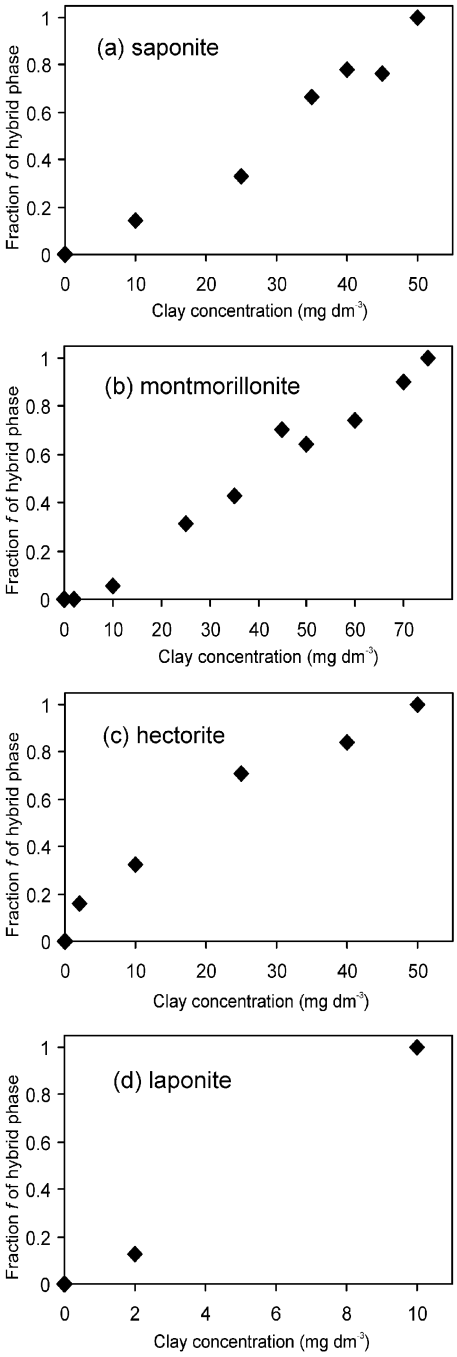

Fig. 4 Fraction f of the hybrid organo-clay phase in coexistence with the fraction $(1 - f)$ of the organic phase of the RhB18 monolayer on clay mineral dispersions of (a) saponite, (b) montmorillonite, (c) hectorite and (d) laponite.

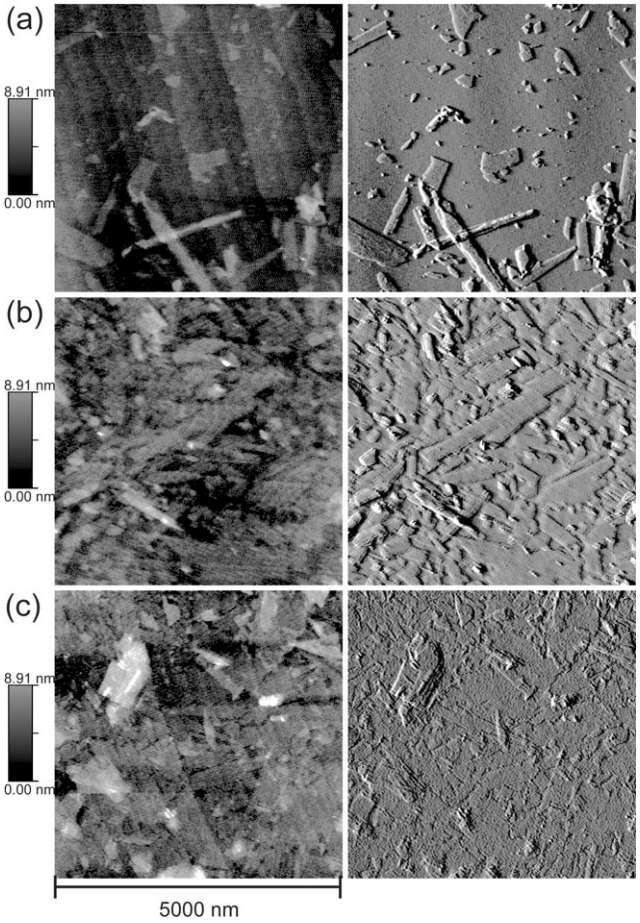

Fig. 5 Atomic force microscopy topography image (left) and cantilever deflection image (right) of OXA18–saponite LB monolayers prepared on a saponite dispersion with a clay concentration of (a) 10 mg dm^{-3}, (b) 50 mg dm^{-3} and (c) 250 mg dm^{-3}. The size of each image is 5000 × 5000 nm.

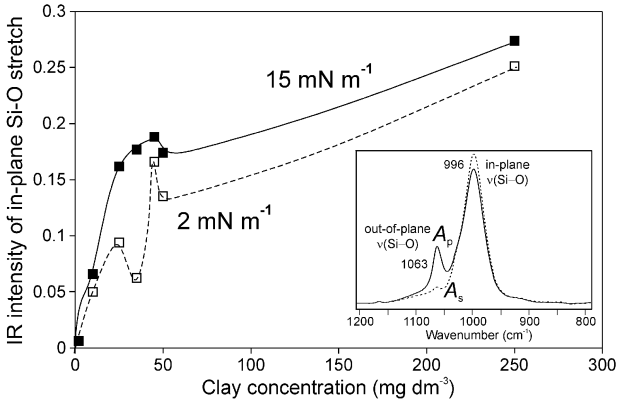

Fig. 6 s-polarized ATR-FTIR intensity of the in-plane Si–O stretch, ν(Si–O), of saponite in hybrid RhB18 monolayers as a function of clay concentration of the dispersion. The s- and p-polarized spectrum of the Si–O stretch region of saponite are shown in the inset.

The trend is the same as at 15 mN m^{-1}, except that the maximum is around 50 mg dm^{-3}.

The same picture emerges when one plots the intensity of the 1590 cm^{-1} band against the amount of clay in dispersion (Fig. 7b). The maximum in the intensity of the 1590 cm^{-1} band corresponds with the maximum in molecular density, both at 15 mN m^{-1} and at 2 mN m^{-1}. The dip in the intensity of the 1590 cm^{-1} band of a film obtained at 2 mN m^{-1} corresponds with the dip in the 996 cm^{-1} band of clay in Fig. 6.

The RhB18 chromophore absorbs around 575 nm and the spectra are shown in Fig. 8. The intensity of the spectrum increases with increasing clay concentration in the dispersion to reach a maximum around 50 mg dm^{-3} and 35 mg dm^{-3} for surface pressures of respectively 2 mN m^{-1} and 15 mN m^{-1}. The increase in intensity is accompanied with a shift of the maximum to higher wavelength. The band shift is indicative for several species contributing to the spectrum or for a change in the polarity of the local environment. Although we cannot exclude a polarity effect, the results in this paper provide evidence for the presence of monomer species and dimer species of RhB18. The integrated area of the UV-Vis band from 450 nm to 650 nm (Fig. 7c) increases and decreases with clay concentration in the same way as the molecular density and the intensity of the 1590 cm^{-1} band. Even the dip at 35 mg dm^{-3} is still present, but much less pronounced than for

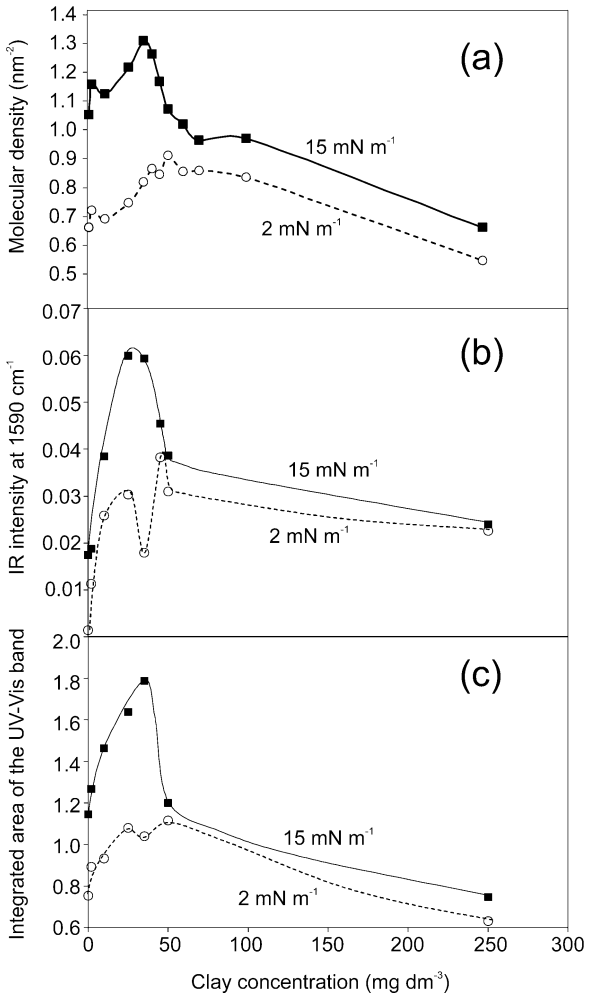

Fig. 7 (a) Molecular density data of RhB18–saponite monolayers extracted from *Π–a* isotherms. (b) ATR-FTIR intensity with s-polarized light of the chromophore band at 1590 cm^{-1} of RhB18–saponite monolayers. (c) Integrated area of the UV-Vis band of RhB18-saponite monolayers.

the Si–O vibration of saponite and the 1590 cm^{-1} band of the RhB18 cation.

3.7. RhB18 dimers

The RhB18 UV-Vis spectrum of Fig. 8 can be decomposed into 3 components: the spectrum of the monomer with maximum at 567 nm; that of a H-dimer with maximum around 540 nm and that of a J-dimer with maximum around 583 nm. H-dimers have a sandwich-type of geometry, *i.e.* the chromophore part of the two molecules are in parallel planes.[27] J-dimers have a linear-type of geometry, *i.e.* the chromophores are in the same plane. Dimers with an intermediate geometry show band splitting into both the 540 nm and 583 bands, as proposed by the exciton theory.[28] When the monomer spectrum is subtracted from the overall spectrum of Fig. 8, the spectra of the dimers are obtained (the subtraction method is explained in Materials and methods). These dimer spectra are shown in Fig. 9. Films prepared on water (0 mg dm^{-3}) show bands at 540 nm and 583 nm. It indicates that monolayers without clay minerals have aggregates present with a geometry intermediate between that of perfect H- and J-dimers, or it indicates that dimers with a range of geometries exist. The films containing clay minerals show an increase in the J-dimer band only; the H-dimer band at 540 nm remains nearly constant. The intensity of the J-dimer band increases with amount of clay minerals in the dispersion to reach a maximum at 50 mg dm^{-3} and 35 mg dm^{-3} for surface pressures of respectively 2 mN m^{-1} and

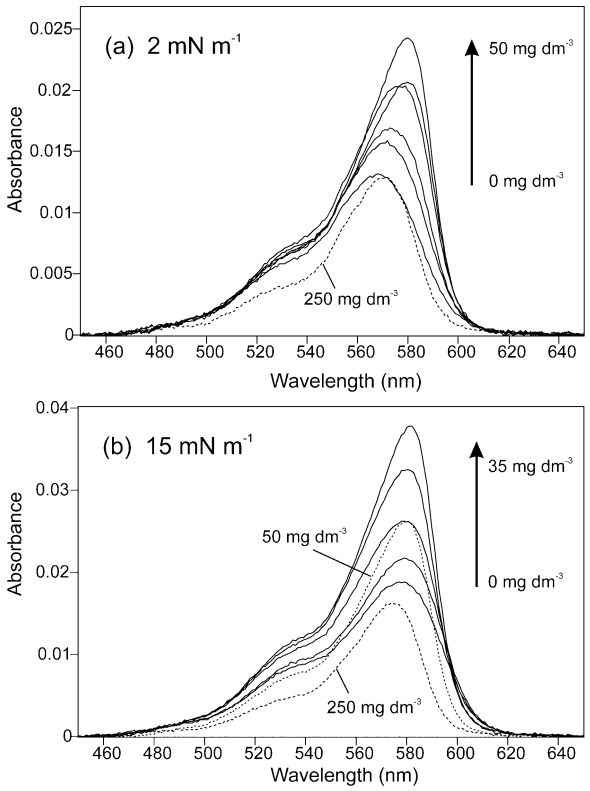

Fig. 8 UV-Vis absorption spectra of RhB18–saponite films deposited at a surface pressure of (a) 2 mN m^{-1} and (b) 15 mN m^{-1} .

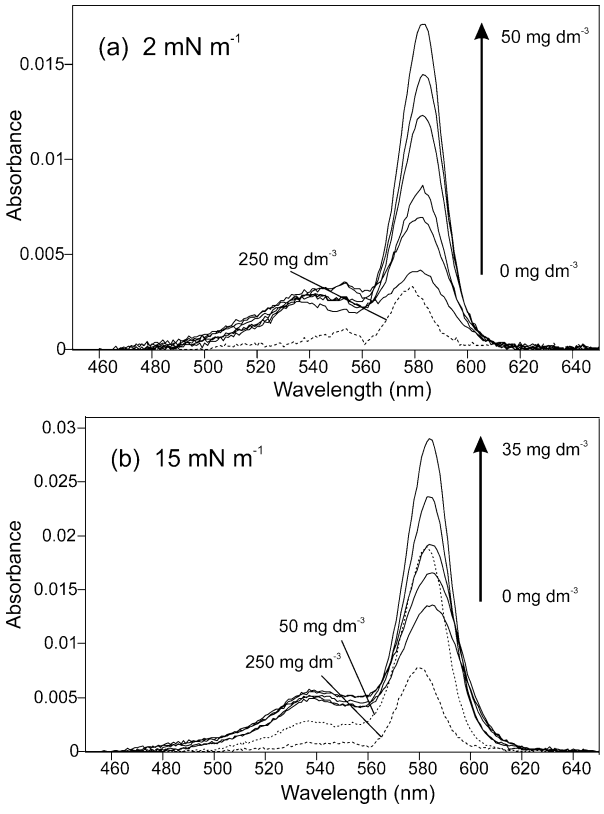

Fig. 9 Calculated dimer spectra of RhB18–saponite films deposited at a surface pressure of (a) 2 mN m^{-1} and (b) 15 mN m^{-1} .

15 mN m^{-1}. These clay concentrations correspond to those films consisting of a pure hybrid clay film with maximum RhB18 density (see Fig. 7). At concentrations larger than 50 mg dm^{-3} less dimers are present in the films. These films also have reduced RhB18 density (see Fig. 7).

This journal is © The Owner Societies 2004

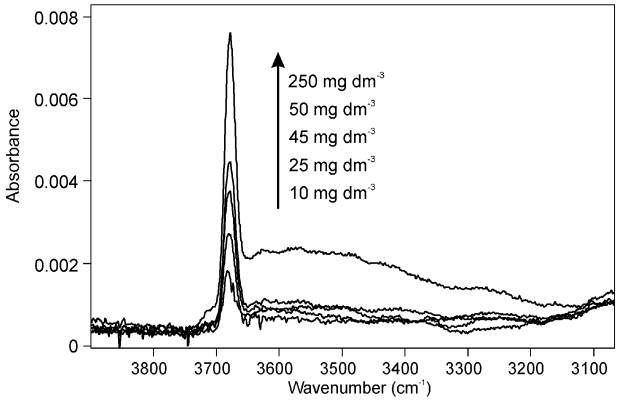

Fig. 10 p-Polarized ATR-FTIR spectra of RhB18–saponite films deposited at 2 mN m^{-1} showing the OH stretch of the structural hydroxyl groups at 3680 cm^{-1} and the OH vibrations of adsorbed water.

3.8. Water in the films

The infrared spectra of RhB18–saponite films from 3900 cm^{-1} to 3100 cm^{-1} are shown in Fig. 10. The narrow band at 3680 cm^{-1} is the OH stretch, ν(OH), of the structural hydroxyl groups of saponite.[17] The broad band from 3700 cm^{-1} to 3200 cm^{-1} is attributed to OH vibrations of adsorbed water.[29] This band is clearly visible in the films prepared on the 250 mg dm^{-3} saponite dispersions, whereas it is significantly reduced at lower clay concentrations. Thus, films formed on 250 mg dm^{-3} saponite dispersions have a significantly higher water content than the films prepared at lower clay concentrations. This must be related to the nearly complete ion-exchange of hydrated Na^+ by RhB18 in films prepared at low clay concentrations, and to the incomplete ion-exchange and the presence of clay particle aggregates in the film prepared on 250 mg dm^{-3} saponite dispersions.

3.9. X-ray reflectivity

X-rays reflecting from a layered film produce an interference pattern due to the successive layers of contrasting electron density, and the pattern can be fit to a surface-normal density profile with sub-Ångstrom resolution. Fig. 11 shows the synchrotron X-ray reflectivity data for LB films of OXA18 and OXA18–saponite on silicon. Both samples were found to have rough surfaces, with the specular reflection progressively broadened along the rocking curve at large q_z (not shown). Similar behaviour has been found for bare silicon surfaces,[30] and thus the base roughness we observe is probably characteristic of the substrates. Nevertheless, X-ray reflectivities measured from the films showed clear oscillations which can be directly related to the length scales of the regions occupied by the clay minerals and dye molecules. The experimental data are shown as symbols in Fig 11(a). The LB film without clay minerals exhibits minima that arise from interference between X-rays reflecting from the air–OXA18 and OXA18–silicon interfaces. The data can be fit by a smoothly varying density dependence at the interface, as shown in Fig 11(b). A second length scale is evident in the data from the OXA18 film containing clay minerals, and successful models show a well defined 1.4 nm thick region between the substrate and OXA18. This region is slightly thicker than the 0.96 nm thickness of a clay mineral lamella, and is also less dense, indicating a partial coverage perhaps accompanied by slight tipping of the clay mineral lamellae or the presence of a small amount of clay aggregates. However, a complete film more than one clay mineral lamella thick is ruled out by the data. Both with and without the saponite, the OXA18 molecules at the surface seem disordered, with no observable difference in OXA18 organization between the two. Dashed lines in Figs. 11(a) and 11(b)

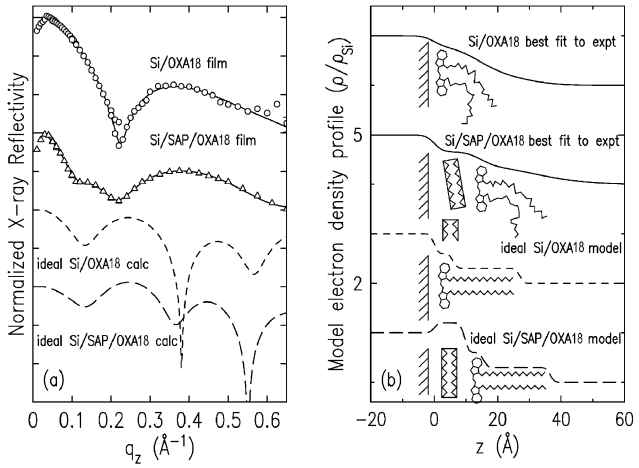

Fig. 11 (a) Fresnel-normalized reflectivity data for silicon/OXA18 film (circles) and silicon/saponite/OXA18 film (triangles). (Data are offset along a logarithmic axis.) Solid lines are calculated for the best fit model profiles. Short and long dash lines are calculated for idealized films where the OXA18 molecules are well ordered with straight hydrocarbon tails. (b) Model real-space electron density profiles (normalized to the substrate density ρ_{Si}). Solid lines correspond to the experimental data, and dashed lines to idealized films, as depicted in the schemes.

demonstrate the differences between our experiment and idealized film structures, in which the saponite particles perfectly tile the surface, and the OXA18 molecules stand straight up and are densely packed. In such models, the minima in the reflectivity are shifted to lower q_z since the straightened molecules define a thicker film.

Our observations demonstrate that the clay particles lie between the OXA18 and the substrate in a well defined single layer, and that the OXA18 molecular tails do not stand straight from the surface. OXA18 is adsorbed on one side of the clay mineral lamella only.

4. Discussion

All the data presented in this paper come qualitatively together in the model of Section 3.3. With increasing amount of clay in the dispersion a monolayer is formed at the air–water interface consisting of an organic phase and a hybrid organo-clay phase. The fraction of the hybrid phase increases with clay concentration of the dispersion until a complete hybrid monolayer is obtained at a typical clay concentration. Above this clay concentration the clay content in the film still increases but the molecular density of the cationic dyes decreases. This model raises additional questions and has consequences that will be discussed below.

In dilute aqueous dispersions the Na^+ smectites are completely swollen, giving a dispersion with clay mineral lamellae about 1 nm thick. These particles have Brownian motion and—to a first approximation—move randomly and independently of each other. When cationic amphiphilic molecules are spread over the water surface, clay mineral lamellae near the air–water interface are attracted and form a hybrid organo-clay film at the air–water interface by a cation-exchange mechanism. This process is easier/faster for the smallest clay particles. We have indeed observed that the concentration of the clay mineral dispersion needed for the hybrid monolayer of laponite is only 10 mg dm^{-3}, less than for the natural clay minerals hectorite, saponite and montmorillonite ($\sim$50 mg dm^{-3}). Two questions are still unresolved: (1) are the smallest particles preferentially picked up from a dispersion with a distribution of particle sizes, such as the dispersions under study here? (2) are the particles moving up towards the air–water interface due to the electrostatic attraction against gravitational force or are only those particles which happen to

be at or close to the air–water interface immobilized at the air–water interface by the cationic surfactants? The answer to the first question can only be given by working with dispersions of particles of the same shape and size and charge density. However, in the AFM image we do see particles of different sizes and shapes. Thus, a preference for the smallest particles only has not been observed. The answer to the second question is also indirect. Umemura *et al.* observed that LB films could be made from dilute clay mineral dispersions and water-soluble alkylammonium cations.[31] This indicates that the rate of ion-exchange at the air–water interface competes favourably with the dissolution rate of the alkylammonium cations. This observation is in favour of the idea that clay mineral particles are electrostatically attracted to the air–water interface, as required by the ion-exchange mechanism.

The data of this paper suggest that dispersions containing single clay mineral lamellae and no aggregates can be prepared from Na^+ smectites. The amount of clay minerals in the dispersion should be smaller than or equal to 50 mg dm^{-3}. With these dilute dispersions hybrid monolayers are formed. According to X-ray reflectivity measurements the structure of the hybrid films is such that the organic cations are adsorbed on one side of the clay mineral lamella only. In between the clay mineral lamella and the substrate no organic cations are present. This observation is likely regarding the asymmetric structure of surfactant monolayers at the air–water interface.

When the deposition of the monolayer is performed on the ZnSe internal reflection element, only low amounts of water are detected in the films. This is indirect proof for the absence of Na^+ ions. The presence of Na^+ indeed immediately involves hydration water. The consequences of this observation are extremely important. (i) The cationic surfactants, being located on the topside of the clay mineral lamellae, have essentially replaced all Na^+ ions of the clay particle. (ii) There are no water molecules between the hybrid clay film and the ZnSe crystal. (iii) The topside of the hybrid film, carrying the cationic surfactants is strongly hydrophobic. All water is expelled by the RhB18 cations.

Further evidence for the replacement of all exchangeable cations on the topside of the clay mineral surface by the cationic surfactant molecules in films made on dispersions with clay concentrations lower than or equal to 50 mg dm^{-3} comes from (i) the one-to-one correspondence between the minimum lift-off area (MLA) and the surface charge density of the four investigated clay minerals (see Table 2) and from (ii) the linear increase in fraction f of clay-containing hybrid phase with increasing clay concentration (see Fig. 4). Because the surfactant density on the clay mineral surface is higher than on the water surface, a spontaneous migration process must exist in which surfactant molecules move from the water surface onto the clay mineral surface to fill all the charge sites of the clay mineral (see Fig. 12).

Clay mineral films formed from dispersions with clay concentrations more than $\sim$50 mg dm^{-3} have some stacks of clay mineral particles incorporated. We presume that in the interlamellar space of the stacks hydrated Na^+ ions are present. Indeed, water is observed in these films. These films also show a reduced density of surfactant molecules, which implies that unexchanged hydrated Na^+ ions are still present. The lower molecular density is caused by the fact that, due to the high clay concentration in the dispersion, the hybrid film is almost instantly formed, fixing the amphiphilic dye cations at their density on the water surface. In this reasoning, the organic phase is negligibly small or non-existing (Fig. 12).

The addition of clay minerals in the films results essentially in an increasing amount of RhB18 J-dimers. The maximum amount of J-dimers is present in the films with the highest surfactant density, both at low and high surface pressure. The film prepared at a saponite concentration of 50 mg dm^{-3}, which is considered to consist of one hybrid phase with all original Na^+ ions exchanged by RhB18, has a J-dimer content nearly independent of the applied surface pressure. It shows that RhB18 molecules are immobilized by the adsorption at the clay mineral surface. In the films that consist of two coexisting phases ($<$50 mg dm^{-3} saponite dispersion) both the surfactant density and the amount of J-dimers increase significantly with increasing surface pressure. Thus, the applied surface pressure causes (i) compacting of the pure organic phase and (ii) forced migration of RhB18 molecules from the pure organic phase onto the clay mineral surface, leading to J-dimers. The molecular density in these films (up to 1.3 nm^{-2}) is higher than the charge density of saponite (0.88 nm^{-2}), suggesting that the clay particles are becoming over-exchanged. These additional RhB18 molecules are not adsorbed by a cation-exchange process and thus it implies that they should have a counterion present. Regarding the structure of a J-dimer it shows that, even at high surfactant density, the RhB18 molecules in the films are located next to each other in one plane and not sandwiched on top of each other as for H-dimers.

In general, cationic dyes preferentially form H-dimers in aqueous solution and in dilute aqueous clay mineral dispersions.[32–36] Those dimers are broken down upon removal of

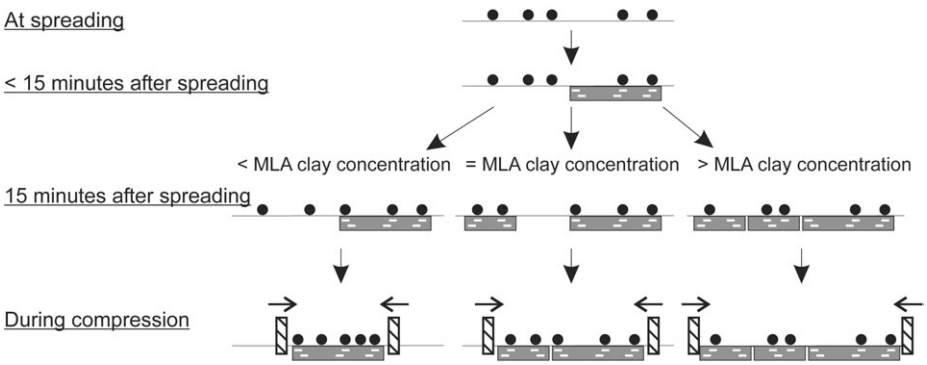

Fig. 12 Schematic representation of the hybrid film formation showing the organization of surfactant molecules (circles) and clay mineral lamellae (rectangles) at the air–water interface when cationic surfactants are spread on a clay mineral dispersion. At $<$ or at the minimum lift-off area (MLA) clay concentration, the surfactant molecules migrate spontaneously from the organic phase onto the clay mineral surface to replace all exchangeable Na^+ ions. After 15 min at the MLA clay concentration, the clay adsorption is sufficiently fast to form a hybrid organo-clay phase where all Na^+ ions are replaced by surfactant. At $<$ MLA clay concentration, an organic phase coexists with the hybrid phase. At $>$ MLA clay concentration, all surfactant molecules have adsorbed on clay before they could migrate spontaneously to the clay mineral surface, resulting in lower surfactant densities. Compression of the films at $>$ MLA clay concentration let the clay particles form a dense layer, but does not significantly alter the molecular density. Compression of the films at MLA clay concentration results in a monolayer completely covered with clay mineral lamellae and the molecular density corresponds to the surface charge density of the clay mineral. Compression of the films at $<$ MLA clay concentration, let the organic phase be pushed over the clay mineral surface to occupy areas in between the charge sites. These films show high surfactant densities.

This journal is © The Owner Societies 2004

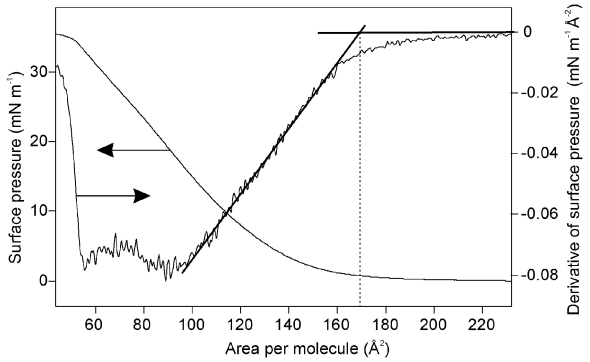

Fig. 13 Π–a isotherm of RhB18 on pure water (left axis) and its derivative (right axis). The lift-off area is determined as 168 Å^2 by extrapolation of the linear section of the derivative.

water.[36] This means that the dominant interactions in water are of the dye–dye type, while at low water content dye–surface interactions become dominant. The latter is the situation in the LB films of the present study. The J-dimers are simply a consequence of the high molecular density at the clay mineral surface.

The surface charge density of clay minerals is shown in this work to determine the density of cationic surfactant molecules in the monolayer. The orientation of the RhB18 chromophore in the hybrid clay films will be discussed in a subsequent paper.[37] The molecular organization (*e.g.*, alkyl chain conformation,[38,39] dye aggregation,[32–34,40] dye orientation[41–44]) in other types of organo-clay complexes have been reported to depend on the surface charge density as well.

5. Conclusion

Hybrid monolayers of cationic surfactant molecules and smectite-type clay minerals are successfully prepared with the Langmuir–Blodgett technique. As the amount of clay minerals in the aqueous dispersion is increased, the amount of clay mineral lamellae in the hybrid films increases until the hybrid film is fully covered with clay minerals. The hybrid monolayers are characterized by a minimum lift-off area (MLA), which is proportional to the average area per charge on the clay mineral surface. This strongly suggests that the film formation is due to an ion-exchange reaction at the air–water interface in which Na^+ is exchanged by surfactant. The MLA determination might be suitable for measuring the surface charge density of clay minerals. Under conditions of MLA and low surface pressure, the molecular density of the hybrid films is maximal, as was confirmed by ATR-FTIR and UV-Vis spectroscopy. At high clay concentrations in the dispersion, the films have a lower density of cationic surfactant and contain aggregates of clay mineral particles and residual water molecules.

Appendix

Lift-off area determination of hybrid monolayers and monolayers containing complex surfactants

The lift-off area of Π–a isotherms can give information about the average size of surfactant molecules[45] and in this work it is shown that a relationship exists between the lift-off area of hybrid clay monolayers and the area per charge on the clay mineral particle. Gaines proposed a method to determine the lift-off area of monolayers consisting of surfactants such as carboxylic acids.[45] These simple surfactants have isotherms with a straight section characteristic for the solid or condensed phase. Gaines' method exists in extrapolation of this straight section to 0 mN m^{-1}. Complex surfactants, such as RhB18, do not show a straight section in the isotherm and it is difficult, if not impossible, to determine the lift-off area *via* this method.

A new method is proposed to determine lift-off areas from the Π–a isotherm. The method consists of taking the derivative of the isotherm as shown in Fig. 13. A linear section in the derivative is observed where the Π–a isotherm starts to lift-off. The extrapolation of this linear section to 0 mN m^{-1} Å^{-2} is taken as the lift-off area.

Acknowledgements

R.H.A.R. would like to thank Dr R. Puurunen for proposing the method for the lift-off area determination, for help with creating the schematic representation of the hybrid film formation and for useful comments on scientific writing of the abstract. This research is financially supported by the Fund for Scientific Research—Flanders through grant G.0201.02 and the bilateral agreement Flanders—Hungary through grant BIL 00/10 and partly by an IAP program on "Supramolecular Chemistry and Catalysis". The NSLS is supported by the USDOE under contract DE-AC02-98CH10886.

References

1 H. Fuchs, H. Ohst and W. Prass, *Adv. Mater.*, 1991, **3**, 10–18.
2 A. N. Shipway, E. Katz and I. Willner, *ChemPhysChem*, 2000, **1**, 18–52.
3 M. Ogawa and K. Kuroda, *Chem. Rev.*, 1995, **95**, 399–438.
4 G. Schulz-Ekloff, D. Wohrle, B. van Duffel and R. A. Schoonheydt, *Microporous Mesoporous Mater.*, 2002, **51**, 91–138.
5 P. Gomez-Romero, *Adv. Mater.*, 2001, **13**, 3516–3523.
6 J. H. Fendler, *Chem. Mater.*, 1996, **8**, 1616–1624.
7 E. R. Kleinfeld and G. S. Ferguson, *Science*, 1994, **265**, 370–373.
8 B. van Duffel, R. A. Schoonheydt, C. P. M. Grim and F. C. De Schryver, *Langmuir*, 1999, **15**, 7520–7529.
9 S. W. Bailey, *Am. Miner.*, 1980, **65**, 1–7.
10 N. A. Kotov, F. Meldrum, J. H. Fendler, E. Tombácz and I. Dékány, *Langmuir*, 1994, **10**, 3797–3804.
11 K. Inukai, Y. Hotta, M. Taniguchi, S. Tomura and A. Yamagishi, *J. Chem. Soc., Chem. Commun.*, 1994, **8**, 959–959.
12 E. Tamura, H. Setsuda, M. Taniguchi and A. Yamagishi, *Langmuir*, 1999, **15**, 6915–6920.
13 E. Tamura, H. Setsuda, M. Taniguchi, T. Nakamura and A. Yamagishi, *Chem. Lett.*, 1999, **2**, 121–122.
14 Y. Umemura, A. Yamagishi, R. Schoonheydt, A. Persoons and F. De Schryver, *Langmuir*, 2001, **17**, 449–455.
15 Y. Umemura, A. Yamagishi, R. Schoonheydt, A. Persoons and F. De Schryver, *J. Am. Chem. Soc.*, 2002, **124**, 992–997.
16 Y. Umemura, Y. Onodera and A. Yamagishi, *Thin Solid Films*, 2003, **426**, 216–220.
17 R. H. A. Ras, C. T. Johnston, E. I. Franses, R. Ramaekers, G. Maes, P. Foubert, F. C. De Schryver and R. A. Schoonheydt, *Langmuir*, 2003, **19**, 4295–4302.
18 J. A. B. Ferreira and S. M. B. Costa, *Phys. Chem. Chem. Phys.*, 2003, **5**, 1064–1070.
19 F. López Arbeloa, J. Martínez Martínez, J. Bañuelos Prieto and I. López Arbeloa, *Langmuir*, 2002, **18**, 2658–2664.
20 S. Banerjee and D. Y. Li, *Appl. Spectrosc.*, 1991, **45**, 1047–1049.
21 E. Vuorimaa, M. Ikonen and H. Lemmetyinen, *Chem. Phys.*, 1994, **188**, 289–302.
22 G. Biesmans, M. Van der Auweraer and F. C. De Schryver, *Langmuir*, 1990, **6**, 177–285.
23 E. Balnois, S. Durand-Vidal and P. Levitz, *Langmuir*, 2003, **19**, 6633–6637.
24 A. Dietrich, H. Möhwald, W. Rettig and G. Brezesinki, *Langmuir*, 1991, **7**, 539–546.
25 R. H. A. Ras, J. Németh, C. T. Johnston, I. Dékány and R. A. Schoonheydt, *Thin Solid Films*, in press.
26 M. Pospíšil, P. Čapková, H. Weissmannová, Z. Klika, M. Trchová, M. Chmielová and Z. Weiss, *J. Mol. Model.*, 2003, **9**, 39–46.
27 I. López Arbeloa and P. Ruiz Ojeda, *Chem. Phys. Lett.*, 1982, **87**, 556–560.
28 M. Kasha, H. R. Rawls and M. Ashraf El-Bayoumi, *Pure Appl. Chem.*, 1965, **11**, 371–392.
29 J. Madejová and P. Komadel, *Clays Clay Miner.*, 2001, **49**, 410–432.
30 A. Gibaud, N. Cowlam, G. Vignaud and T. Richardson, *Phys. Rev. Lett.*, 1995, **74**, 3205–3208.

31 Y. Umemura, A. Yamagishi, R. Schoonheydt, A. Persoons and F. De Schryver, *Thin Solid Films*, 2001, **388**, 5–8.
32 J. Bujdák, M. Janek, J. Madejová and P. Komadel, *J. Chem. Soc., Faraday Trans.*, 1998, **94**, 3487–3492.
33 M. G. Neumann, F. Gessner, C. C. Schmitt and R. Sartori, *J. Colloid Interface Sci.*, 2002, **255**, 254–259.
34 K. Y. Jacobs and R. A. Schoonheydt, *J. Colloid Interface Sci.*, 1999, **220**, 103–111.
35 K. Y. Jacobs and R. A. Schoonheydt, *Langmuir*, 2001, **17**, 5150–5155.
36 B. van Duffel, K. Y. Jacobs and R. A. Schoonheydt, in *Proceedings of the 11th International Clay Conference*, ed. H. H. Kodawa, Ottawa, 1997, pp. 475–481.
37 R. H. A. Ras, J. Németh, C. T. Johnston, I. Dékány and R. A. Schoonheydt, *Phys. Chem. Chem. Phys.*, submitted.
38 G. Lagaly, *Layer charge determination by alkylammonium ions*, in *Layer charge characteristics of 2:1 silicate clay minerals*, ed. A. R. Mermut, vol. 6 of *CMS Workshop Lectures*, The Clay Minerals Society, Boulder, Colorado, 1994, pp. 1–46.
39 R. A. Vaia, R. K. Teukolsky and E. G. Giannelis, *Chem. Mater.*, 1994, **6**, 1017–1022.
40 S. Takagi, T. Shimada, M. Eguchi, T. Yui, H. Yoshida, D. A. Tryk and H. Inoue, *Langmuir*, 2002, **18**, 2265–2272.
41 T. Endo, T. Sado and M. Shimida, *J. Phys. Chem. Solids*, 1986, **47**, 799–804.
42 M. Iwasaki, M. Kita, K. Ito, A. Kohno and K. Fukunishi, *Clays Clay Miner.*, 2000, **48**, 392–399.
43 D. Fischer, W. R. Caseri and G. Hähner, *J. Colloid Interface Sci.*, 1998, **198**, 337–346.
44 N. Iyi, R. Sasai, T. Fujita, T. Deguchi, T. Sota, F. L. Arbeloa and K. Kitamura, *Appl. Clay Sci.*, 2002, **22**, 125–136.
45 G. L. Gaines Jr., *Insoluble monolayers at liquid-gas interfaces*, John Wiley & Sons, 1966.
46 http://cms.lanl.gov/chem.htm.
47 H. Suquet, C. de la Calle and H. Pezerat, *Clays Clay Miner.*, 1975, **23**, 1–9.
48 D. A. Laird, A. D. Scott and T. E. Fenton, *Clays Clay Miner.*, 1989, **37**, 41–46.
49 N. Willenbacher, *J. Colloid Interface Sci.*, 1996, **182**, 501–510.

 This journal is © The Owner Societies 2004